



Synthesis of Polar Dielectric Barium Magnesium Niobate at Low Sintering Temperature: Dielectric Relaxation and AC Conductivity Study

K. N. Singh¹ and P. K. Bajpai^{2*}

¹*Department of Physics, OP Jindal University, Raigarh (C.G.) India.*

²*Advance Materials Research Laboratory, Department of Pure and Applied Physics, Guru Ghasidas Vishwavidyalaya, Bilaspur, Chhattisgarh-495009, India.*

Authors' contributions

This work was carried out by author KNS as a part of Ph.D. program under the mentorship of author PKB. Author PKB designed the study, wrote the protocol and wrote the first draft of the manuscript.

Author KNS synthesized the material and performed the experiments. Both authors PKB and KNS analyzed the data and managed the analyses of the study. Both authors read and approved the final manuscript.

Article Information

DOI: 10.9734/PSIJ/2017/37111

Editor(s):

- (1) Shi-Hai Dong, Department of Physics School of Physics and Mathematics National Polytechnic Institute, Mexico.
(2) Thomas F. George, Chancellor / Professor of Chemistry and Physics, University of Missouri-St. Louis, Boulevard St. Louis, USA.

Reviewers:

- (1) Aruna P. Maharolkar, Marathwada Institute of Technology, India.
(2) Yong X. Gan, California State Polytechnic University, USA.

Complete Peer review History: <http://www.sciencedomain.org/review-history/21595>

Original Research Article

Received 1st October 2017
Accepted 20th October 2017
Published 27th October 2017

ABSTRACT

$Ba(Mg_{1/3}Nb_{2/3})O_3$ is an important microwave polar dielectric material. However, the large leakage current and losses due to defects incorporated during high temperature processing restricts its use in microwave devices. We have synthesized phase pure perovskite $Ba(Mg_{1/3}Nb_{2/3})O_3$ by controlling the cooling rates during calcination and sintering, using two stage columbite method at relatively low sintering of 1150 C. X-ray diffraction has been used to determine the structural details. Ceramics stabilizes in hexagonal perovskite structure with lattice constant $a=5.7803\text{\AA}$, $c=7.0780\text{\AA}$. Sintered ceramics with density > 93% exhibit surface morphology having homogeneous grain distribution with average grain size is $\approx 1.0\text{-}2.0\ \mu\text{m}$. Temperature and frequency dependent dielectric response has been analyzed to understand the dielectric dispersion. Dielectric response is temperature independent up to $\approx 180^\circ\text{C}$. Beyond this temperature

*Corresponding author: E-mail: bajpai.pk1@gmail.com;

dielectric dispersion is observed which is more pronounced at lower frequencies and associated with significant electrical conductivity. Impedance spectroscopic formalism has been used to separate out the contributions from grains and grain boundary using equivalent circuit approach, whereas, electrical modulus approach has revealed the role of conductivity relaxation. The frequency/ temperature dependent ac conductivity suggests conduction being thermally activated process. AC conduction activation energies are estimated from Arrhenius plots and conduction mechanism is discussed.

Keywords: Dielectric relaxation; polar dielectrics; X-ray diffraction; impedance analysis.

1. INTRODUCTION

Niobium-based complex perovskite oxides $A(B'_{1/3}Nb_{2/3})O_3$ have attracted attention due to their promising electrical and electro-mechanical properties [1–4]. These oxides crystallize either in a disordered cubic structure or in a hexagonally ordered structure. The ordered structure stems from the 1:2 ordering of B-site cations along the [1-11] direction of the cubic perovskite cell. In many of these complex perovskites, dielectric loss depends on the degree of ordering [5]. Recently, dielectric properties of niobium based ceramics [6-10] are reported as lead free compositions for polar dielectric applications.

Barium magnesium niobate (BMN) is a polar dielectric and a potential material for microwave dielectric applications due to its high Q factor and high dielectric constant at microwaves frequencies [12-13]. BMN based ceramics have been targeted to find alternate for the Ta-based complex perovskite ceramics such as $Ba(Mg_{1/3}Ta_{2/3})O_3$ because of the expensive Ta_2O_5 . However, BMN has been reported to have comparatively higher dielectric loss than corresponding tantalate $Ba(Mg_{1/3}Nb_{2/3})O_3$ (BMT) [14]. Another major problem in using BMN has been the high sintering temperature to reach a satisfactory final density [4,5]. Thus, reducing sintering temperature and dielectric losses in the material remains a challenge. Further, low frequency dielectric dispersion observed in the ceramics could not be understood through impedance formalism due to marked electrical conductivity. The use of the electric modulus formalism gives insight into the bulk response and is effective in case of ceramics with significant electrical conductivity. This is due to the fact that the local behavior of the defects can be separated from electrode effects in electric modulus representation [10,12]. Such an approach allowed us to overcome the difficulties caused by high electrical conductivity, which can mask the dielectric relaxation processes.

We have recently synthesized ceramics with smaller dielectric loss by reducing the sintering temperature in a number of phase pure perovskites by optimizing the process parameters [15-17]. It is thus expected that process parameters optimization during synthesis may lead to phase pure BMN at relatively lower sintering temperature, in turn reducing the dielectric loss.

In this work, we report the synthesis of $Ba(Mg_{1/3}Nb_{2/3})O_3$ in pure perovskite phase with reasonably high density (>93%) at relatively low sintering temperature of 1150°C without using any additives/sintering aids. This has been achieved by simply controlling the rate of cooling and heating during sintering. Structural, dielectric and electrical properties have been probed using impedance and electrical modulus approach.

2. EXPERIMENTAL DETAILS

$Ba(Mg_{1/3}Nb_{2/3})O_3$ ceramics was synthesized by two steps solid state reaction (columbite route). In the first step, pre-reacting Nb_2O_5 (99.9 % Loba Chemie Pvt. Ltd., India) with MgO (99.5 % Loba Chemie Pvt. Ltd., India), forms columbite phase $MgNb_2O_6$ [18]. The calcination was performed in an alumina crucible at 1100°C for 6 h. Phase formation in calcined powder has been checked by x-ray diffraction. The prepared columbite phase is then reacted with $BaCO_3$ in an alumina crucible at 1125°C for 6h. The ceramic powder so obtained was structurally analyzed using x-ray diffraction (Rigaku Miniflex). The fine and homogeneously calcined powder was pressed into cylindrical pellets of 10 mm diameter and 1-2 mm thickness under a uniaxial pressure of 3×10^6 N/m² using a hydraulic press. Polyvinyl alcohol (PVA, 1 mole % solution) was used as a binder to reduce the brittleness of the pellets. The pellets were fired first at 500°C to remove the binder and then sintered at 1150°C for 6 hours. The heating and cooling rates were controlled during sintering by varying temperature ramp from 3°C/min to 1°C/min in a microcontroller controlled muffle furnace. Phase

purity and densification were simultaneously checked after each sintering carried at different temperature ramp applied during cooling and heating cycle of sintering process. Experimental density was measured using Archimedes method and verified by direct pellet weight measurement.

Finally, the phase pure ceramics having experimental density >93% were obtained when sintered at 1150°C with lowest ramp rate. The sintered pellets were electroded with silver paste, heated at 500°C for 1 hour and cooled down to room temperature before electrical measurements were performed. The dielectric and impedance data were measured in the temperature range 30-350°C using HIOKI 3532 LCR Hi TESTER. The temperature was measured with an accuracy of $\pm 1^\circ\text{C}$ using a μP controlled temperature controller interfaced with the LCR Hi-Tester. Microstructural features were studied using scanning electron microscopy (SEM, Carl Zeiss).

3. RESULTS AND DISCUSSION

3.1 Structural and Microstructural Characterization

Fig. 1 depicts the room temperature X-ray diffraction (XRD) pattern in the 2θ range from 20-80° of sintered BMN pellet that shows the highest percentage density.

All the observed peaks were indexed using a least-squares method with the help of a standard Powder X-ray diffraction interpretation and indexing program (POWD). The unit cell is selected for which the observed and calculated d-values $\sum \Delta d = \sum (d_{\text{obs}} - d_{\text{cal}})$ is minimum. Good agreement between the observed and calculated

inter-planar spacing (d-values) is obtained for perovskite hexagonal phase. The refined lattice parameters values ($a=5.7803\text{\AA}$, $c=7.0780\text{\AA}$) and X-ray diffraction pattern are in close agreement with earlier report (JCPDF No-17-0173). X-ray diffraction data confirms the formation of single phase. The results of indexing are summarized in Table 1.

We have varied sintering conditions by varying the sintering time and cooling rates after sintering. Even though XRD patterns observed remains same, the microstructure varies significantly as the sintering time is varied. Fig. 2 (a-c) shows the SEM micrographs of the gold coated pellets sintered for different duration and at different cooling rates after sintering; changing the sintering duration changes the microstructure showing different types of grain distribution and grain packing, porosity and agglomeration.

The best microstructure is achieved for material having the highest value of percentage density of 5.767 gm/cm^3 ($\approx 93\%$ of theoretical density) under the conditions; sample sintered for 30 hours at 1150°C and keeping the cooling rate of 1°C/min after sintering. Average grain size is $\approx 1.0\text{-}2.0\ \mu\text{m}$ as estimated by linear intercept method. Percentage experimental density is measured by Archimedes method at different sintering temperatures; the densification is very sensitive to sintering temperature. Relative density of the material decreases when sintered above 1150°C (density variation with sintering temperature not shown for the sake of brevity). This may be due to the defects generated (mainly oxygen vacancies) during high temperature processing may leads to anion deficient phase and / or produce distortion in $\text{B/B}'\text{O}_6$ octahedron reducing the densification.

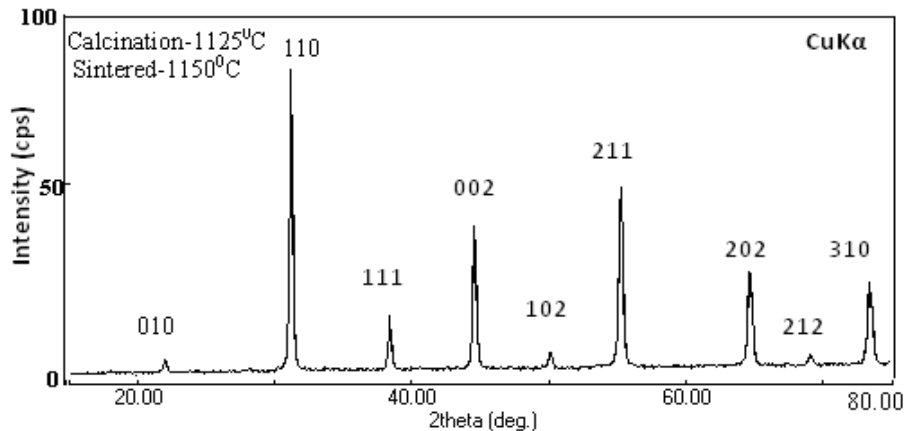


Fig. 1. X-ray diffraction pattern of $\text{BaMg}_{1/3}\text{Nb}_{2/3}\text{O}_3$ (BMN) at room temperature

Table 1. Observed and calculated d- values in (Å) of some reflection of BMN at room temperature with observed relative intensity (I/I_0)

d-spacing(obs.)	d-spacing(cal.)	Intensity	h	k	l
4.0804	4.0800	9	1	0	1
2.8930	2.8930	100	1	0	2
2.3571	2.3570	20	2	0	1
2.0445	2.0450	42	2	0	2
1.8273	1.8270	10	1	1	3
1.6681	1.6680	52	1	0	4
1.4450	1.4450	29	2	0	4
1.3619	1.3620	9	1	0	5
1.2325	1.2320	26	2	0	5

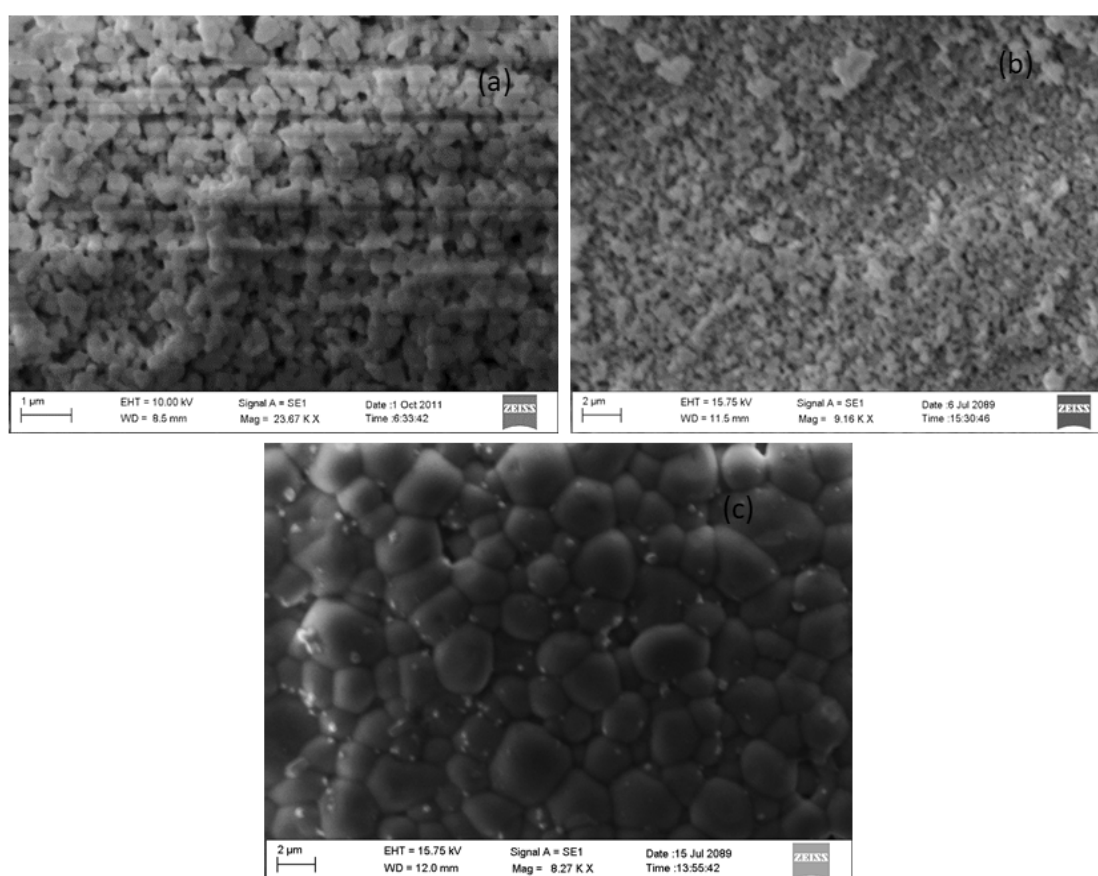


Fig. 2. SEM micrographs of sintered powders of BMN calcined at 1125°C and sintered at 1150°C (a) sintered for 8 hours and cooling rate 2°C per minute after sintering, (b) sintered for 16 hours with cooling rate 1°C per minute after sintering and (c) sintered for 30 hours with a cooling rate of 1°C

3.2 Dielectric Studies

The ordered perovskites are characterized by a temperature-independent dielectric response in the low frequency range ($< 10^9$ Hz). Fig. 3

exhibits the temperature variation of dielectric constant (ϵ') and tangent loss (in the inset) at representative frequencies. Material shows frequency independent- very low loss ($\tan\delta$) dielectric response up to $\approx 180^\circ\text{C}$.

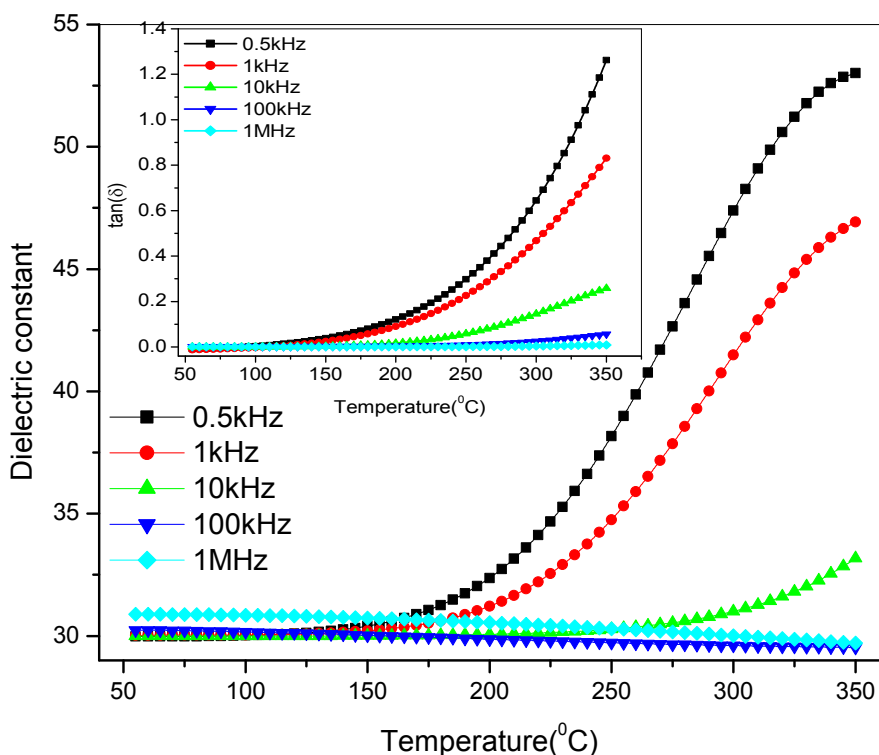


Fig. 3. Temperature variation of dielectric constant (ϵ'). Inset shows temperature dependence of tangent loss

The values of dielectric permittivity increase with further increase in temperature. The increase in dielectric response, particularly at high temperature and low frequencies may be due to interfacial polarization [19]. At low temperatures, the molecule cannot orient themselves in polar dielectrics. As the temperature rises, the dipoles reorient and contribute to dielectric response. Thus, at higher temperatures, the dielectric loss due to the dipole mechanism increases and reaches to a maximum value as the degree of dipole orientation increases [20]. The increase in both components of dielectric permittivity at temperatures $> 180^{\circ}\text{C}$ may be associated to this phenomena [21].

The frequency dependence of real (ϵ') and imaginary (ϵ'') parts of dielectric permittivity at different temperatures are shown in Fig. 4(a) and 4(b) respectively.

Dielectric constant (ϵ') gradually decreases as the applied ac field frequency is increased from a value of 55 at 0.5 kHz. The dispersion increases with increasing temperature suggesting that ac conductivity in BMN is due to bulk effect [22]. The low frequency dispersion in Fig. 4(a)

indicates the absence of any inhomogeneity arising owing to Maxwell-Wagner polarization.

Complex dielectric response as a function of the frequency ω has been explained by Jonscher's universal power law [23] as

$$\epsilon^* = \epsilon' - j\epsilon'' = \epsilon_{\infty} + \frac{\sigma}{\epsilon_0 \omega} + (\alpha(T)/\epsilon_0) \omega^{n(T)-1} \quad (1)$$

where ϵ_{∞} is the high frequency value of the dielectric constant, $n(T)$ is the temperature dependent exponent and $\alpha(T)$ determines the strength of the polarizability arising from the universal mechanism in question. Experimental data were fitted in equation (1) to obtain the values of parameters $n(T)$, and $\alpha(T)$, at different temperatures. The $\alpha(T)$ value increases from 6.7×10^{-13} to 2.7×10^{-8} , whereas $n(T)$ value decreases from 0.82 to 0.19 as the temperature increased from room temperature up to 350°C . The interaction between the charge carriers contributing in the polarization process is characterized by $n(T)$; its value decreases with increase in temperature indicating strengthened dipolar interaction at higher temperatures. Frequency dispersion of ϵ'' gives two slopes, almost close to -1 in the low frequency region

(DC conduction) and the one with a slope (n-1) in the high frequency region associated with hopping assisted localized conduction (Fig. 4(b)). In the present case, the range of frequency region having slope (-1) increases as the temperature is increased indicating that at higher temperatures dc conduction dominates the conduction process.

3.3 Impedance Studies

In order to understand the role of extrinsic factors in the charge transport process and to separate out grains and grain boundaries contribution to the conduction, complex impedance analysis is performed. Impedance spectroscopy may be a better tool to understand the relaxation process than the dielectric analysis. The grains and grain boundaries may be represented in terms of series combination of two equivalent circuit of parallel RC network, each giving rise to semicircular arc in complex impedance plane, Z^* [23] where

$$Z^* = Z' - Z'' \quad (2)$$

With $Z' = \frac{R}{1+(\omega RC)^2}$ and $Z'' = \frac{\omega RC}{1+(\omega RC)^2}$. Therefore, in the impedance formalism, grains and grain boundaries contribution could be separated out.

Fig. 5 shows the variation of real part of impedance (Z') with frequency at representative temperatures.

The magnitude of Z' decreases with the increase in both frequency as well as temperatures; above

60 kHz it becomes temperature independent. This may be due to the release of space charge [24,25]. Inset of Fig. 5 shows the variation of Z'' with frequency at different temperatures. Impedance loss (Z'') peak starts appearing at temperatures $\geq 300^\circ\text{C}$ with asymmetric broadening. The peak shifts towards higher frequency with increasing temperature due to the spread of relaxation times and increasing loss in the sample. The (Z'') peak heights are proportional to bulk (R_b) according to equation:

$$Z'' = R_b \left[\frac{\omega\tau}{1+\omega^2\tau^2} \right] \quad (3)$$

Probably, high temperature triggers grain boundary relaxation process as evident from the asymmetric broadening of the peaks [26]. The relaxation frequency (frequency at loss peak maximum, ω_m) obeys the Arrhenius relation given by $\omega_m = \omega_0 \exp[-E\tau/k_B T]$, where ω_0 is a pre-exponential factor, k_B is Boltzmann constant and T is temperature in absolute Kelvin. The calculated activation energy for the corresponding relaxation process is 0.43 eV.

Complex impedance plots (Z'' vs. Z') at different temperatures are shown in Fig. 6, it could be fitted with double semicircle inferring that the impedance contribution arising from both gains and grain boundaries.

Estimated values of equivalent circuit parameters considering representing resistance and capacitance of grains (R_g, C_g) and grain boundaries (R_{gb}, C_{gb}) using non-linear fitting program (Zsimpwin) are shown in Table 2.

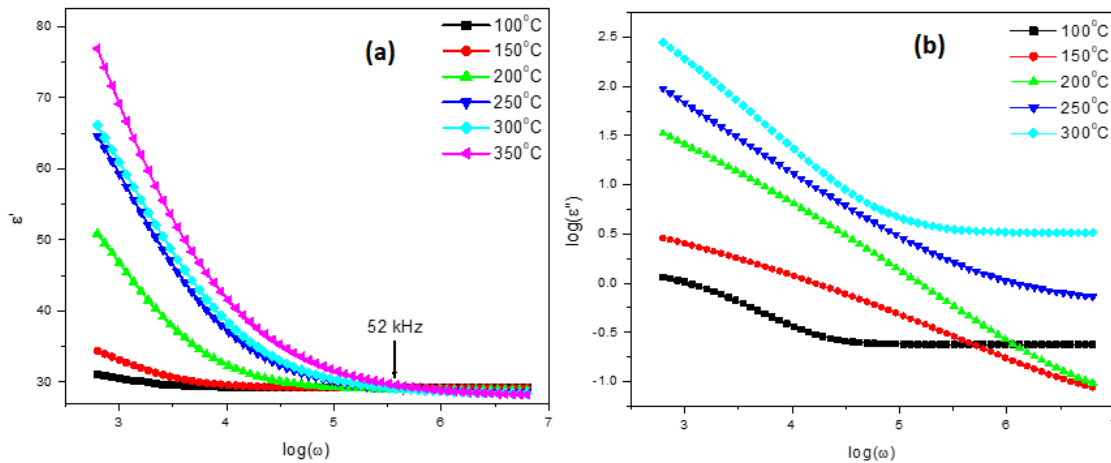


Fig. 4. Frequency dependence of (a) real (ϵ') part of dielectric constant and (b) imaginary (ϵ'') part of dielectric constant on a log-log scale

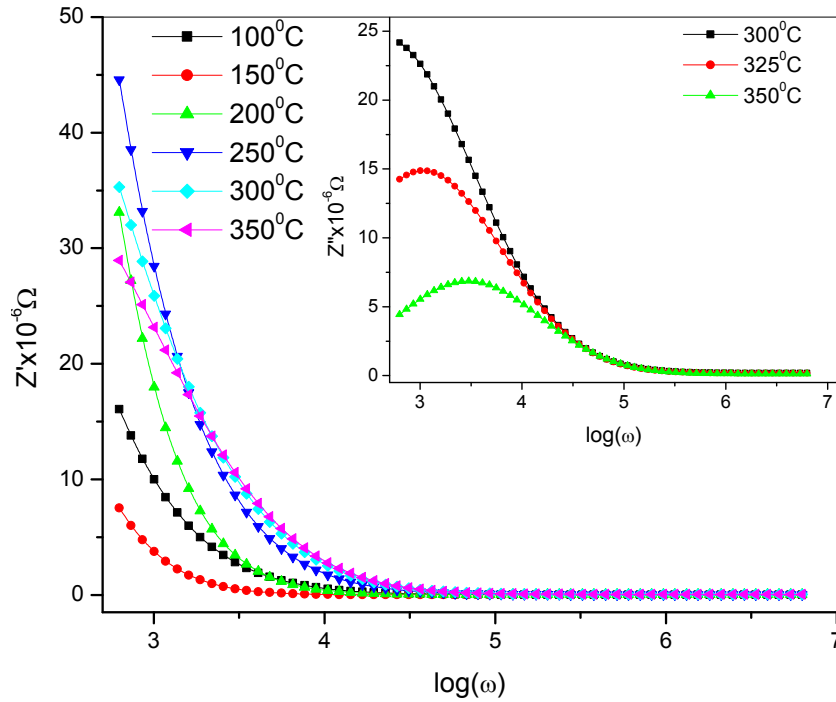


Fig. 5. Frequency variation of real part of impedance (Z'). Inset shows the frequency dependence of Z''

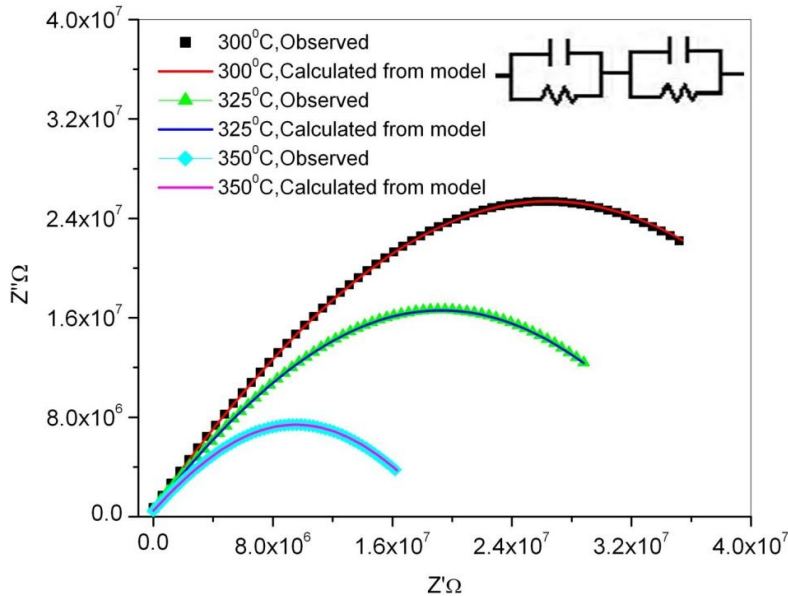


Fig. 6. Nyquist plot (Z' vs. Z'') along with the non-linear least square (NLLS) fitting results (solid lines), using equivalent circuit model as shown in the figure

From the Table 2, it is clear that the ceramic possesses highly resistive grain boundaries at room temperature; the transport through grains and grain boundaries is thus thermally activated since R_g and R_{gb} both decreases with increase in temperature. The material shows negative

temperature coefficient of resistivity like semiconductors.

3.4 Electric Modulus Study

In the modulus formalism, bulk response is highlighted and electrode effect is suppressed. Therefore, the formalism is useful in understanding the relaxation phenomenon occurred in grains. Electric modulus M^* is defined in terms of the complex dielectric permittivity by [27].

$$M^*(\omega) = M_\infty \left[1 - \int_0^\infty e^{-j\omega\tau} \left(\frac{d\phi(t)}{dt} \right) dt \right] \quad (4)$$

Where the function $\phi(t)$ gives the time evaluation of the electric field within the dielectrics. The electric modulus data can be fitted with the Cole–Cole expression defined as [28]:

$$M' = \frac{M_\infty M_s \{M_s A + (M_\infty - M_s) \cos \phi\} A}{M_s^2 A^2 + 2A(M_\infty - M_s) M_s \cos \phi + (M_\infty - M_s)^2} \quad (5)$$

$$M'' = \frac{M_\infty M_s \{(M_\infty - M_s) \sin \phi\} A}{M_s^2 A^2 + 2A(M_\infty - M_s) M_s \cos \phi + (M_\infty - M_s)^2} \quad (6)$$

Where A and ϕ are given as

$$A = \left[1 + 2(\omega\tau)^{1-\alpha} \sin(\alpha\pi/2) + (\omega\tau)^{2(1-\alpha)} \right]^{1/2} \quad (7)$$

$$\phi = \tan^{-1} \left[(\omega\tau)^{1-\alpha} \cos(\alpha\pi/2) / 1 + (\omega\tau)^{1-\alpha} \sin(\alpha\pi/2) \right] \quad (8)$$

Thus, circular arcs are expected in electric modulus also. The frequency dependence of $M'(\omega)$ are shown in Fig. 7(a); value of M' decreases as the temperature increases. Above 300°C, M' starts from origin at low frequencies, value increases with increase in frequency and gets saturated at higher frequency. This behavior of electric modulus confirms an appreciable electrode and / or ionic polarization contribution to dielectric response [29]. Saturation of M' values at higher temperature may be related to a lack of restoring force governing the mobility of charge carriers. Data exhibit a pronounced relaxation peak for $M''(\omega)$ (Fig.7(b)) that moves towards higher frequencies with increase in temperature. It can be inferred that the process is associated with a single relaxation and further that the relaxation rate for the process increases with increasing temperature. The behavior of observed M'' peak can well be associated with a transition from short range to long range mobility of charge carriers as the frequency decreases.

Towards low frequency side, ions perform hopping successfully between the equivalent neighboring sites, whereas towards high frequency side, ions are confined to the potential wells and execute only localized motion [30-31]. The characteristic relaxation time, the inverse of frequency of the maximum peak position, i.e.

$\tau_m = \omega_m^{-1}$ satisfies Arrhenius law. From the numerical fitting the value of the activation energy comes out to be 0.22 eV. The different values of activation energies obtained impedance (0.43 eV) and electric modulus data (0.22 eV) indicates that different mechanisms are operative in relaxation process.

Table 2. Grain and grain boundary parameters from NLLS fitting, using series combination of parallel RC equivalent circuit model for BMN

Temperature(°C)	R _g (Ω)	C _g (Farad)	R _{gb} (Ω)	C _{gb} (Farad)
100	2.0x10 ⁷	1.9x10 ⁻¹⁰	4.8x10 ⁹	4.9x10 ⁻¹²
125	5.4x10 ⁶	9.4x10 ⁻¹⁰	4.6x10 ⁹	1.5x10 ⁻¹³
150	6.9x10 ⁶	9.4x10 ⁻¹⁰	3.9x10 ⁹	4.5x10 ⁻¹³
175	1.4x10 ⁶	9.4x10 ⁻¹⁰	1.2x10 ⁹	1.6x10 ⁻¹²
200	3.3x10 ⁵	8.0x10 ⁻¹⁰	2.3x10 ⁸	3.5x10 ⁻¹¹
225	3.5x10 ⁵	9.3x10 ⁻¹⁰	1.4x10 ⁸	1.8x10 ⁻¹⁰
250	1.3x10 ⁵	4.3x10 ⁻⁹	9.1x10 ⁸	1.1x10 ⁻¹⁰
275	2.5x10 ⁵	9.2x10 ⁻⁹	9.5x10 ⁶	1.1x10 ⁻¹⁰
300	6.4x10 ⁴	2.2x10 ⁻⁸	4.2x10 ⁴	1.4x10 ⁻¹⁰
325	1.1x10 ⁴	5.3x10 ⁻⁸	5.2x10 ⁴	1.6x10 ⁻¹⁰
350	9.8x10 ³	9.2x10 ⁻⁸	3.9x10 ⁴	1.8x10 ⁻¹⁰

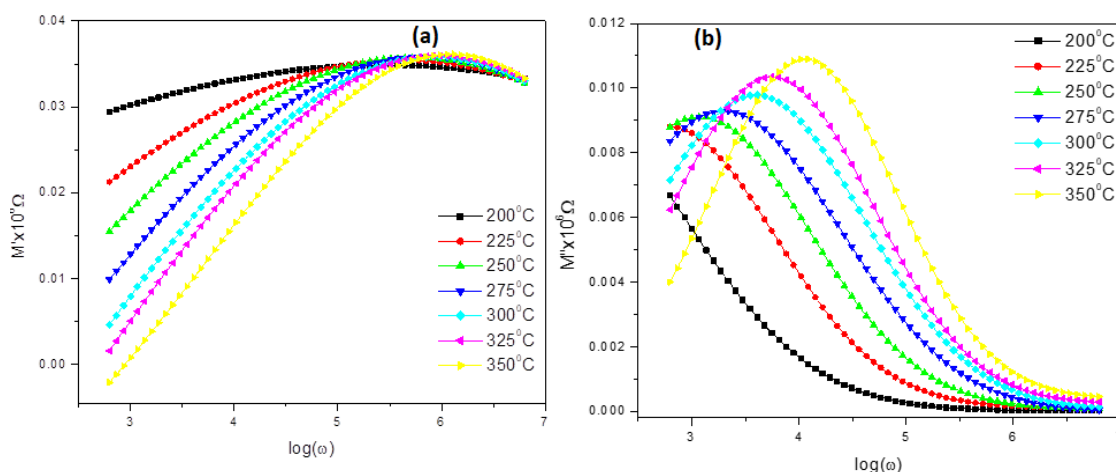


Fig. 7. Frequency dependence at representative temperatures of (a) real part of electric modulus (M') and (b) imaginary part of electric modulus (M'') for BMN

In both the impedance and electric modulus formalism, complex plots exhibit peaks, which are broader than predicted by Debye relaxation and have significant asymmetry. Thus, the observed relaxation is non-Debye type. The associated activation energy for electric modulus and impedance relaxation processes have different values; normalized plots of $M''(\omega)$ and $Z''(\omega)$ peaks show only partial overlapping (figure not shown). These facts suggest the presence of both long range and localized relaxation in the material.

3.5 AC Electrical Conductivity Study

The ac conductivity $\sigma(\omega) = \omega \epsilon_0 \epsilon''$, has been calculated from impedance data. The frequency spectrum of the ac conductivity for BMN is shown in Fig. 8.

The conductivity shows dispersion which shifts to higher frequency side with the increase of temperature. It is seen from figure that σ decreases with decreasing frequency and becomes independent of frequency after a certain value. Extrapolation of this part towards lower frequency limit gives σ_{dc} . The real part of conductivity spectra can be explained by the power law defined as [32,33]:

$$\sigma(\omega) = \sigma_{dc} + A\omega^n \tag{9}$$

Here A is a thermally activated quantity and n is the frequency dependent exponent that takes values < 1. Equation (9) is used to obtain the values of σ_{dc} , A, n by non-linear fitting of ac

electrical conductivity data and the results are shown in Table 3.

Table 3. Non-linear fitting parameters obtained by fitting a c conductivity data in equation (9) for BMN

Temperature (C)	σ_{dc}	A	n
50	6.2×10^{-10}	6.4×10^{-11}	0.49
100	2.2×10^{-9}	2.3×10^{-11}	0.47
150	5.3×10^{-9}	7.6×10^{-9}	0.20
200	7.9×10^{-9}	5.9×10^{-9}	0.19
250	1.3×10^{-8}	9.7×10^{-9}	0.13
300	2.1×10^{-8}	2.6×10^{-9}	0.23
350	1.8×10^{-7}	1.8×10^{-9}	0.29

The values of σ_{dc} as shown in Table 3 are plotted in Arrhenius plot as shown in Fig. 9 which follows Arrhenius law. The linear regression gives activation energy value of 1.1 eV.

Significantly different values of activation energies for relaxation and conduction reveals that the charge species involve in transport are not the one relaxing. Oxygen vacancies are generally considered as major defects in perovskites especially when synthesized through solid state high temperature route. The activation energies for conduction through oxygen vacancies (defect) is typically 0.4-0.5 eV. Thus, very high activation energy involved in DC conduction clearly reflects that DC conduction probably occurs through cation vacancies.

Temperature dependence of ac conductivity at representative frequencies is shown Fig. 10.

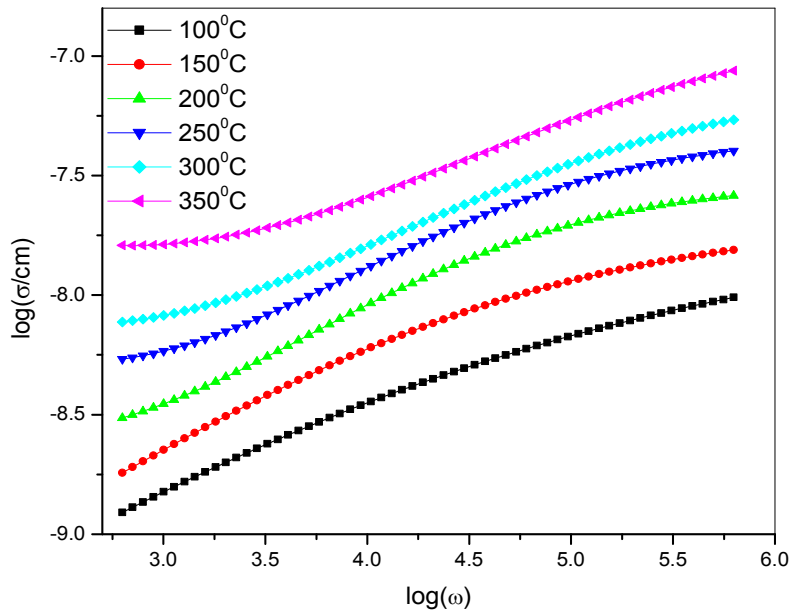


Fig. 8. Frequency spectra of a c electrical conductivity plotted as function of ($\log\omega$) for BMN

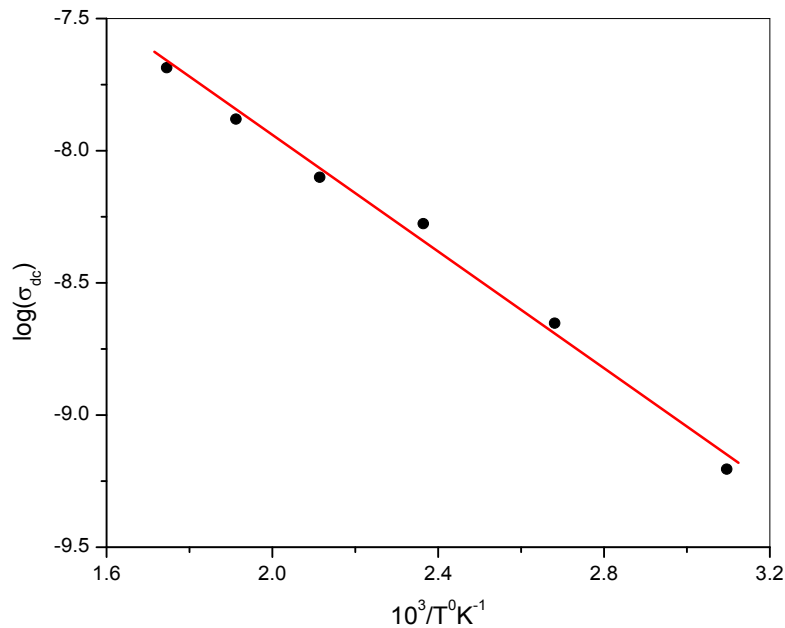


Fig. 9. Arrhenius plot ($\log(\sigma_{dc})$ vs. $10^3/T$) for BMN. The dots are the experimental points and the solid line linear regression fit

As is clear, the ac electrical conductivity is almost temperature independent in the low temperature range; the range becomes smaller as the frequency decreases. However, it increases with increase in temperature and shows significant frequency dependence; an increase by three order of magnitude from kHz to MHz range ($\approx 10^{-10}\sigma/cm$ at 1 kHz to $\approx 10^{-7}\sigma/cm$ at 1MHz). The

temperature dependent conductivity shows NTCR (negative temperature coefficient of resistance) behavior like semiconductors, which is related to the bound carriers trapped in the material [34]. The activation energy values for ac conduction process have been calculated from the slope of the graph (Fig.10) as shown in Table 4.

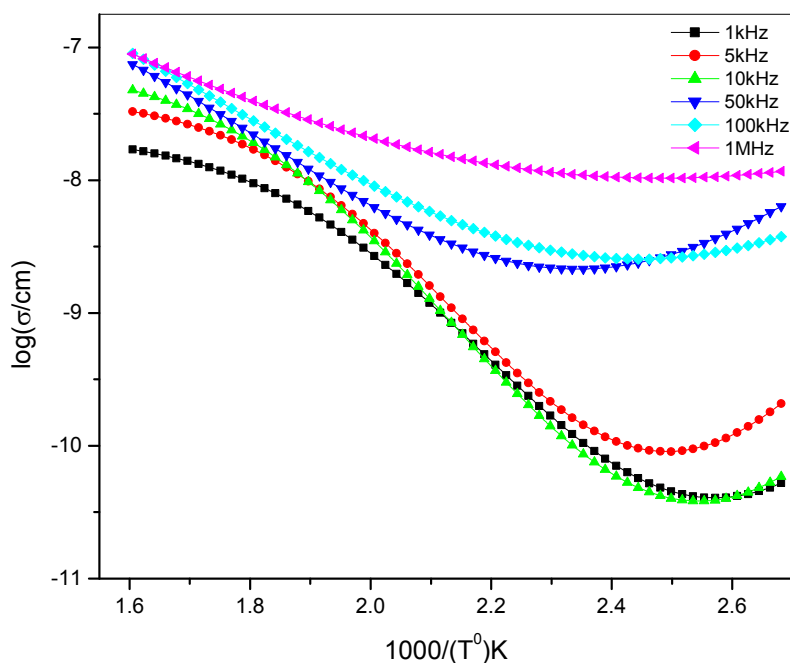


Fig. 10. Temperature dependence of a c electrical conductivity at representative frequencies

Table 4. Activation energies values at different frequencies calculated by linear fitting of temperature dependence of AC conductivity for range of temperature in which the variation is linear

Frequency in (KHz)	Temperature range	
	Activation energy (eV) 100°C to 175°C	Activation energy (eV) 200°C to 350°C
1	0.15	0.20
10	0.06	0.24
100	0.07	0.22
1000	0.08	0.17

The different slope of the plots in the considered temperature range suggested that different mechanisms are operative. In the temperature range (100-175°C), the activation energy varies from 0.15- 0.08eV, whereas at higher temperatures (200-350°C) the activation energy varies from 0.20-0.17 eV.

4. CONCLUSIONS

BMN ceramics, prepared by columbite method, stabilizes in hexagonal perovskite phase with lattice constant $a=5.7803\text{\AA}$, $c=7.0780\text{\AA}$ and average grain size of $1.0\ \mu\text{m}$. By controlling the sintering optimization, ceramics with almost

homogeneous grain distribution and relatively dense packing (>93%) are obtained at significantly low sintering temperature. The observed dielectric dispersion above 180°C is attributed to bulk effect. Dielectric loss spectrum indicates the thermally activated nature of the dielectric relaxation in the system. The relaxation frequency obeys the Arrhenius relation. The activation energy associated with Z" relaxation is 0.43 eV, whereas for electric modulus (M") relaxation it is 0.22 eV, suggesting two different relaxation processes operating in the system. AC conductivity exhibits dispersion at low frequencies and follows Jonscher's power law. σ_{dc} follow Arrhenius law with activation energy is 1.1 eV.

ACKNOWLEDGEMENT

PKB is grateful to University Grants Commission (UGC), India for providing SAP grant and Department of Science & Technology, Govt. of India for providing FIST Grant to the Department of Pure & Applied Physics, GGV, Bilaspur making it possible to perform the work.

COMPETING INTERESTS

Authors have declared that no competing interests exist.

REFERENCES

- Kawashima S, Nishida M, Ueda I, Ouchi H. Ba(Zn_{1/3}Ta_{2/3})O₃ ceramics with low dielectric loss at microwave frequencies. *J. Am. Ceram. Soc.* 1983;66(6):421-423.
- Nomura S, Toyama K, Kaneta K. Ba(Mg_{1/3}Ta_{2/3})O₃ ceramics with temperature-stable high dielectric constant and low microwave loss. *Jpn J. Appl. Phys.* 1982;21(10):L624.
- Desu SB, O'Bryan HM. Microwave loss quality of BaZn_{1/3}Ta_{2/3}O₃ ceramics. *J. Am. Ceram. Soc.* 1985;68 (10):546-551.
- Vincent H, Perrier C, Theritier P, Labeyrie V. Crystallographic study by Reitveld method of barium magnesium tantalite oxide ceramics for use as dielectric resonators. *Mater. Res. Bull.* 1993;28(9): 951-958.
- Liu D, Yao X, Cross LE. Order-disorder and dielectric relaxation in SrFeO_{3-x}. *J. Appl. Phys.* 1992;71(10):5115.
DOI: <http://dx.doi.org/10.1063/1.350615>
- Iguchi E, Hashimoto Y, Kurumada M, Munakata F. Ionic conduction due to oxygen diffusion in La_{0.8}Sr_{0.2}GaO_{3-δ}La_{0.8}Sr_{0.2}GaO_{3-δ} electrolyte. *J. Appl. Phys.* 2003;93(6):3662.
DOI:<http://dx.doi.org/10.1063/1.1555840>
- Gerhardt R. Impedance and dielectric spectroscopy revisited: Distinguishing localized relaxation from long range conductivity *J. Phys. Chem. Solids.* 1994; 55(12):1491-1506.
- Jonscher AK. Near Debye dielectric responses. *J. Phys. D: Appl. Phys.* 1980; 13(5)L89.
- Jonscher AK. Dielectric relaxation in solids: Chelsea Dielectrics Press, London; 1983.
- Jonscher AK. Universal relaxation law: Chelsea Dielectrics Press; London; 1996.
- Reznichenko LA, Geguzina GA, Dergunova NV. Piezoelectric solid solutions based on alkali niobates. *Inorganic Materials.* 1998;34(2):167-173.
- Haussonne JM, Desgardin G, Herve A, Boufrou B. Dielectric ceramics with relaxors and a tetragonal tungsten bronze. *Journal of the European Ceramic Society.* 1992;10(6):437-452.
- Reznichenko LA, Dergunova NV, Geguzina GA, Razumovskaya ON, Shilkina LA, Ivanova LS. NaNbO₃-Based binary solid solutions. *Inorganic Materials.* 1997; 33(12):1277-1284.
- Raevski IP, Prosandeev SA. A new, lead free, family of perovskites with a diffuse phase transition: NaNbO₃-based solid solutions. *J. Phys. Chem. Solids.* 2002; 63(10): 1939-1950.
- Bajpai PK, Singh KN. Dielectric relaxation and ac conductivity study of Ba(Sr_{1/3}Nb_{2/3})O₃. *Physica B.* 2011;406 (6-7):1226-1232.
- Mohan CRK, Bajpai PK. Effect of sintering optimization on the electrical properties of bulk Ba_xSr_{1-x}TiO₃ ceramics. *Physics B.* 404(13):2173-2188.
- Bajpai PK, Pastor M, Singh KN. Relaxor behavior and dielectric relaxation in Pb(Ba_{1/3}Nb_{2/3})O₃: A phase pure new relaxor material. *J. Appl. Phys.* 2011; 109(1):014114.
- Singh KN, Bajpai PK. Synthesis, characterization and dielectric relaxation of phase pure columbite MgNb₂O₆: Optimization of calcination and sintering. *Physica B.* 2010;405(1):303-312.
- Lee HJ, Park HM, Song YW, Cho YK, Nahm S, Byun J-D. Microstructure and dielectric properties of barium strontium magnesium niobate. *J. Am. Ceram. Soc.* 2001;84(9):2105-2110.
- Maharolkar AP, Murugkar AG, Khirade PW, Mehrotra SC. Study of thermophysical properties of associated liquids at 308.15 K And 313.15 K. *Russian Journal of Physical chemistry A (SPRINGER).* 2017;91(9):1710-1716.
- Nomura S. Ceramics for microwave dielectric resonators. *Ferroelectrics.* 1983; 49(1):61-70.
DOI: [doi.org/10.1080/00150198308244666](http://dx.doi.org/10.1080/00150198308244666)
- Dutta A, Bharti C, Sinha TP. Dielectric relaxation and ac conductivity study in SrMg_{1/3}Nb_{2/3}O₃. *Indian Journal of Engineering & Material Sciences.* 2008; 15(2):181-186.
- Jonscher AK, The universal dielectric response. *Nature*, 1977; 267: 673-679.
doi:10.1038/267673a0.
- West AR, Sinclair DC, Hirose N. Characterization of electrical materials, especially, ferroelectrics, by impedance spectroscopy. *J. Electroceramics.* 1975; 1(1):65-71.
- Macdonald J. Ross, impedance spectroscopy: Emphasizing solid materials and systems. Wiley Inter-Science Publications; 1987.
- Maier J. Defect chemistry and ion transport in nanostructured materials: part II:

- aspects of nanoionics. *Solid State IONICS*. 2003;157 (1-4) 327-334.
27. Maier J. Thermodynamics and morphology of nanostructured ion conductors: Aspects of nanoionics Part I. *Solid State Ionics*; 2002;154/155:291-301.
28. Rao KS, Krishna PM, Prasad DM, Effect of simultaneous substitution of Li^+ and Ti^{4+} in ceramics of $\text{Pb}_2\text{KNb}_5\text{O}_{15}$ on structure, dielectric, modulus, impedance and conductivity properties. *Physics Status Solidi (b)*. 2007;244(6)2267-2287. DOI: 10.1002/pssb.200642364
29. Fleig J, Maier J. The polarization of mixed conducting SOFC cathodes: Effects of surface reaction coefficient, ionic conductivity and geometry. *J. Eur. Ceram. Soc.*2004;24(6):1343-1347.
30. Macedo PB, Moynihan CT, Bose R. The role of ionic diffusion in polarization in vitreous ionic conductors. *Physics and Chemistry Glasses*. 1972;13:171-179.
31. Tsangaris GM, Psarras GC, Kouloumbi N. Electric modulus and interfacial polarization in composite polymeric systems. *J. Mater. Sci.* 1998;33(8):2027-2037.
32. Hirose N, West AR. Impedance spectroscopy of undoped BaTiO_3 ceramics. *J. Amer. Ceram. Soc.* 1996; 79(6):1633-1641.
33. Almond DP, West AR. Anomalous conductivity prefactors in fast ion conductors. *Nature (London)*. 1983;306: 456-457.
34. Hairetdinov EF, Uvarov NF, Patel HK, Martin SW. Estimation of the Free Charge Carrier Concentration in Fast Ion Conducting $\text{Na}_2\text{Sb}_2\text{S}_3$ Glasses from an Analysis of the Frequency Dependent Conductivity. *Phys. Rev. B*. 1994;50(18): 13259-13266. DOI: 10.1103/PhysRevB.50.13259

© 2017 Singh and Bajpai; This is an Open Access article distributed under the terms of the Creative Commons Attribution License (<http://creativecommons.org/licenses/by/4.0>), which permits unrestricted use, distribution, and reproduction in any medium, provided the original work is properly cited.

Peer-review history:

The peer review history for this paper can be accessed here:
<http://sciencedomain.org/review-history/21595>